Supporting Information

Bottom-up Approach towards Single-Crystalline VO_2-Graphene Ribbons as Cathodes for Ultrafast Lithium Storage

Shubin Yang[†,§,*], *Yongji Gong*[‡,§], *Zheng Liu*[†], *Liang Zhan*[†], *Daniel P. Hashim*[†], *Lulu Ma*[†], *Robert Vajtai*[†], *Pulickel M. Ajayan*[†,‡,*]

[†]Department of Mechanical Engineering & Materials Science, Rice University, Houston, Texas 77005, USA

[‡]Department of Chemistry, Rice University, Houston, Texas 77005, USA

*E-mail: sy13@rice.edu, ajayan@rice.edu

[§]These authors contributed equally to this work

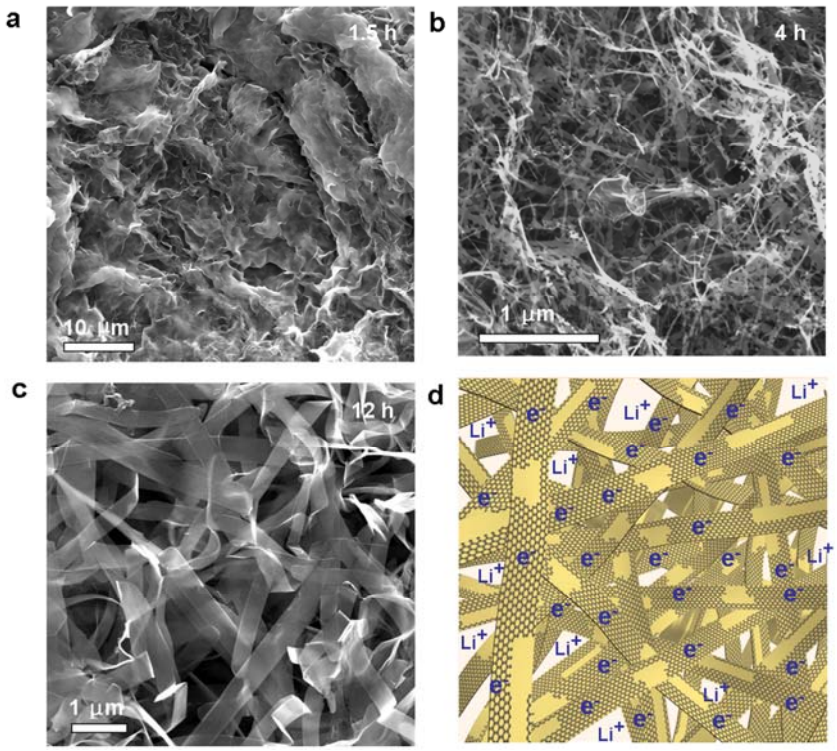

Figure S1. The formation process of VO_2-graphene architectures and applied for lithium storage. **a**, at the initial stage (<1.5h), V_2O_5 was dissolved into water and covered onto the surface of GO sheets. **b**, With the increase of reaction time from 1.5 to 4h, V_2O_5 was partially reduced to irregular ribbons by the functional groups such as phenol and hydroxyl on GO. Meanwhile, the resulting ribbons became building blocks to construct 3D

architectures during the hydrothermal process. Interestingly, the most of GO sheets became invisible at this stage, indicating that GO sheets was unzipped to ribbons along with the formation and crystallization of VO_2 ribbons, which can be demonstrated by the HRTEM images of VO_2 ribbons (incontinuous graphene are coated onto the surface of VO_2 ribbons. **c**, With the further increase of reaction time to 12h, 3D architectures constructed by numerous VO_2 ribbons with thin, flexible and single-crystalline features and incontinuous graphene layers were generated. **d**, Lithium storage in 3D VO_2-graphene architecture (12h), where the electrolyte (light red) fills the pores, facilitating the fast diffusion of lithium ions from electrolyte to the surface of VO_2 ribbons; and the 3D interpenetrating network is favorable for the rapid diffusion of electrons.

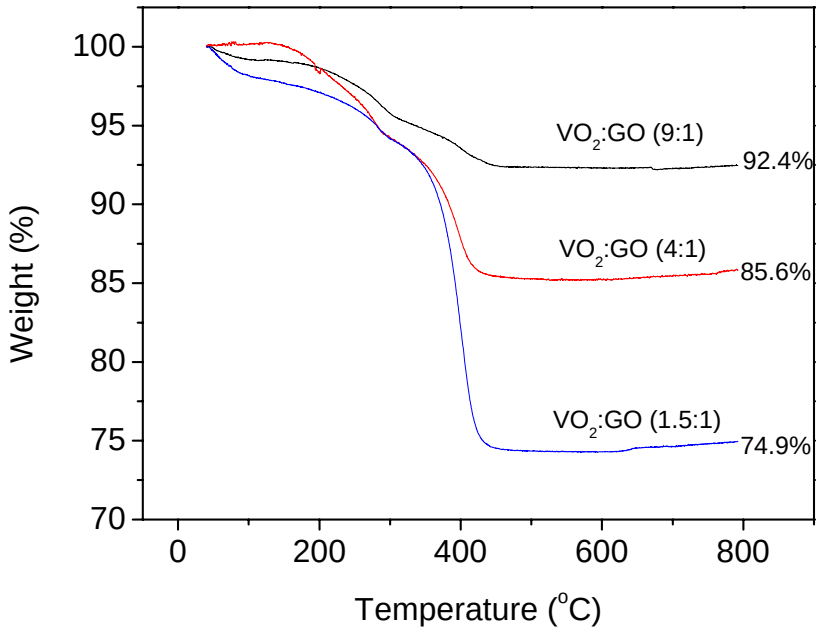

Figure S2. Thermogravimetric analysis (TGA) of VO_2-graphene architectures with different VO_2 contents. The TGA were carried out from 30 to 800 ^oC with the heating rate of 10 ^oC min^{-1} in air. It is indicated that the V_2O_5 residues after TGA tests are 92.4%, 85.6% and 74.9% for the VO_2-graphene architectures synthesized with the different ratio of 9:1, 4:1 and 1.5:1 between V_2O_5 and GO, respectively. Correspondingly, the contents of VO_2 in the three VO_2-graphene architectures are 84%, 78%, 68%, respectively.

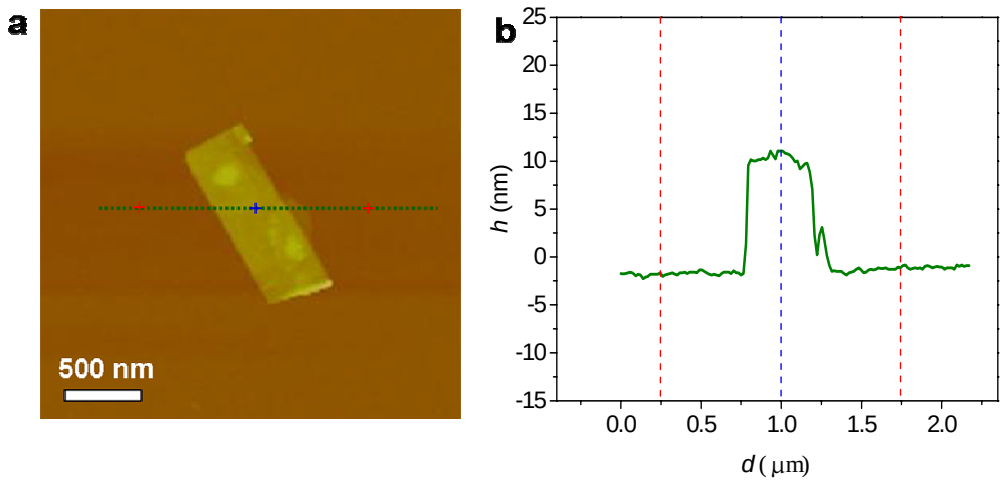

Figure S3. Thickness analysis of VO_2-graphene ribbons. a, Representative AFM images, and **b,** corresponding thickness analysis taken around the green line in (a) reveal a uniform thickness of about 10 nm for the ribbons.

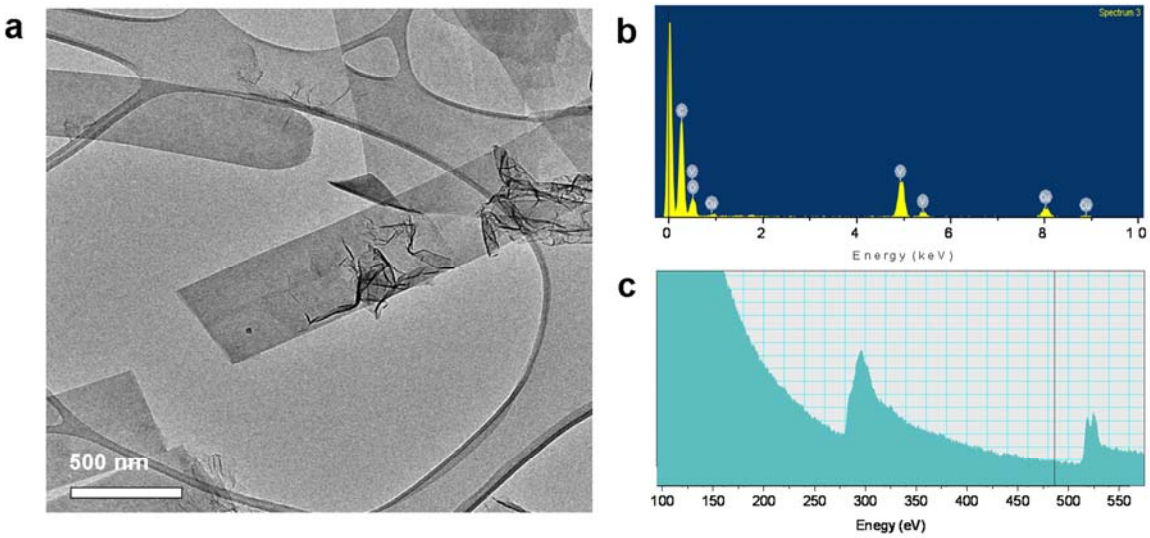

Figure S4. Typical TEM image, EDX and EELS of VO_2 ribbons. a, the TEM image shows several ribbons with the width of 200-600 nm. **b**,**c**, EDS and EELS reveal the co-existence of vanadium, oxygen and carbon in the VO_2 ribbons. The atomic ratio between vanadium and oxygen is about 2:1.

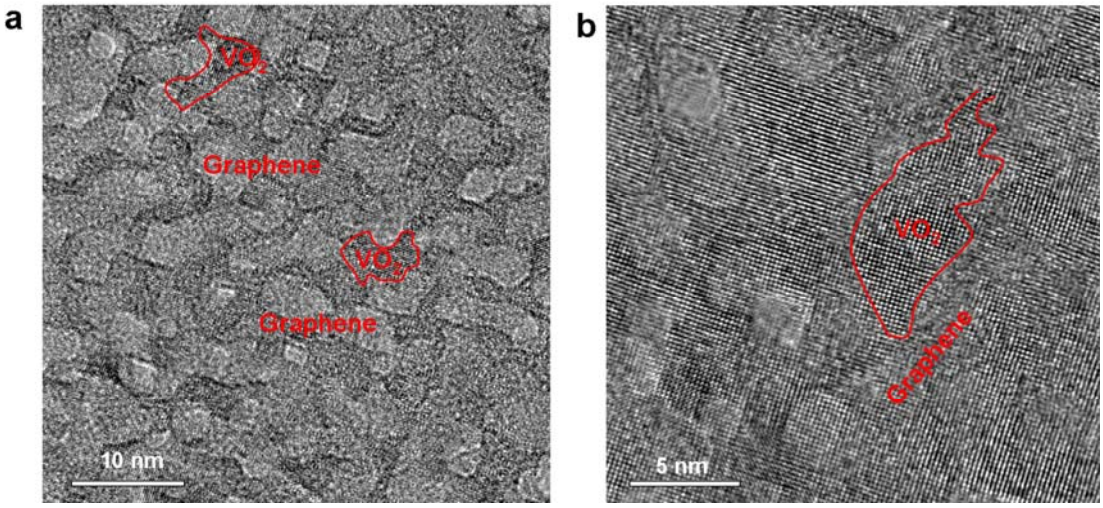

Figure S5. HRTEM images of VO_2 ribbons with different magnifications. a,**b**, HRTEM images show the incontinuous structure of graphene on the surface of VO_2 well-crystalline ribbons. The red line frameworks are shown the exposed single-crystalline VO_2 area.

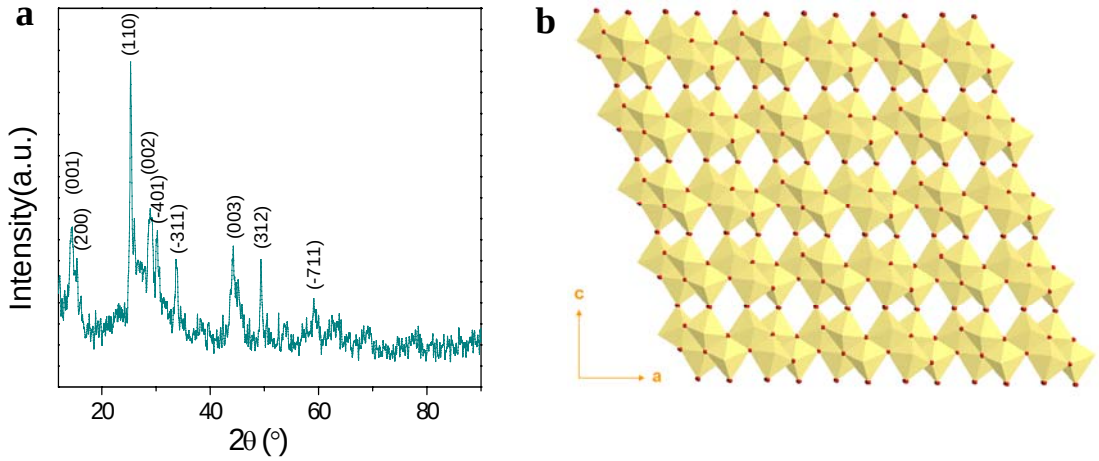

Figure S6. Crystal structure of VO_2-graphene architecture. a, XRD patterns are entirely indexed in the space group C2/m with standard lattice constants a = 12.03 Å , b =3.693 Å, c = 6.42 Å (β =106.6^o) for VO_2(B) with a monoclinic structure. **b**, Structural model of monoclinic VO_2(B) phase projected along [010] facet on the basis of the XRD analysis of (a).

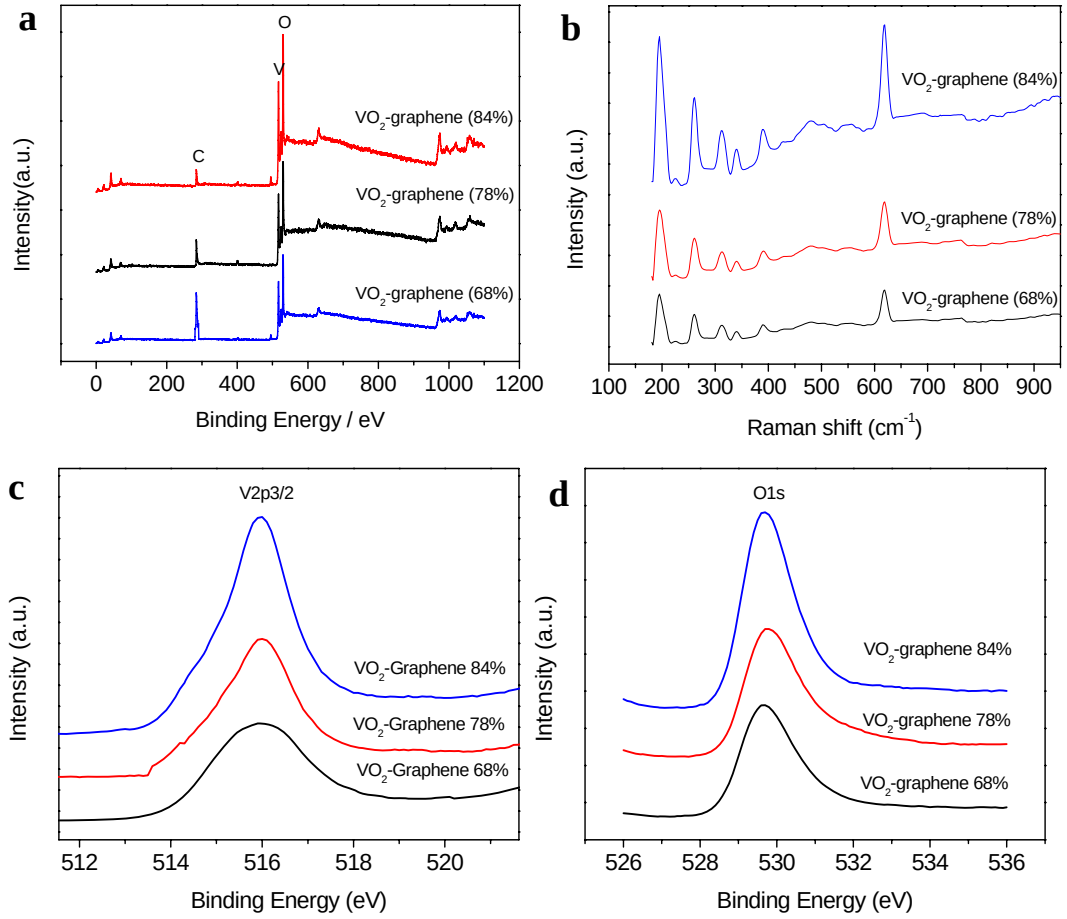

Figure S7. XPS and Raman spectra of VO_2-graphene architectures with different VO_2 contents. a, XPS survey reveal the co-existence of vanadium, oxygen and carbon in all the VO_2-graphene architectures. **b**, Raman spectra of VO_2-graphene architectures with three different VO_2 contents of 84%, 78% and 68%, indicating the monoclinic VO_2(B) phase. Raman spectra at 195, 224, 340, 390, 480 and 618 cm^{-1} correspond to A_g symmetry, and that at 312 cm^{-1} is of B_g symmetry. **c**,**d**, High resolution (e) V2p3/2 and (f) O1s XPS spectra of 3D architectures disclose the ratios between V and O are about 1:2.

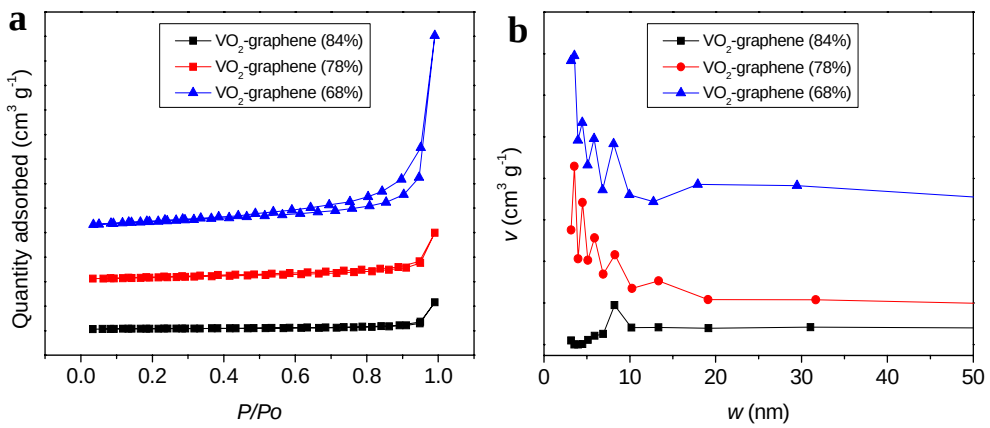

Figure S8. Structural characteristics of VO_2-graphene architectures with different VO_2 contents. a, Nitrogen adsorption/desorption isotherms demonstrate the porous structure with BET surface areas of 405, 156 and 66 m^2 g^{-1} for the VO_2-graphene architectures with the different VO_2 contents of 68.3%, 78.1% and 84.3%, respectively. **b**, Pore size distributions reveal that the pore sizes in VO_2-graphene architectures are in the range of 3-30 nm.

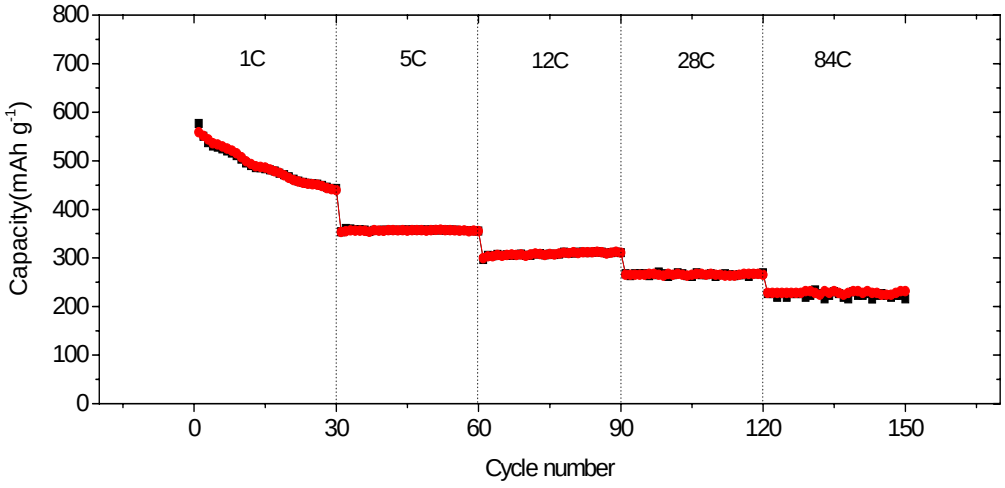

Figure S9. Rate capacities of VO_2-graphene architecture with the VO_2 content of 84% under room temperature, measured for 30 cycles at each selected rate from 1C to 84C.

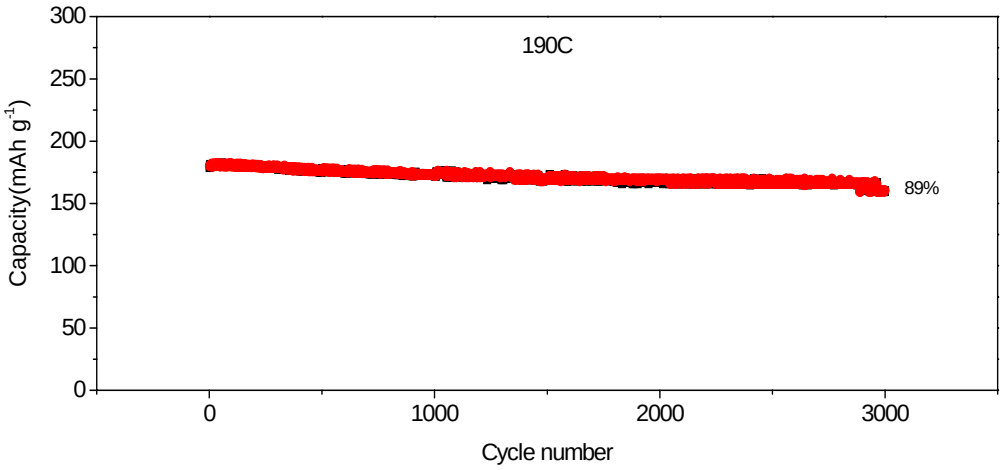

Figure S10. Capacity retention of VO_2-graphene architecture with the VO_2 content of 68% when performing full discharge-charge at the highest rate of 190C for 3000 cycles under room temperature.

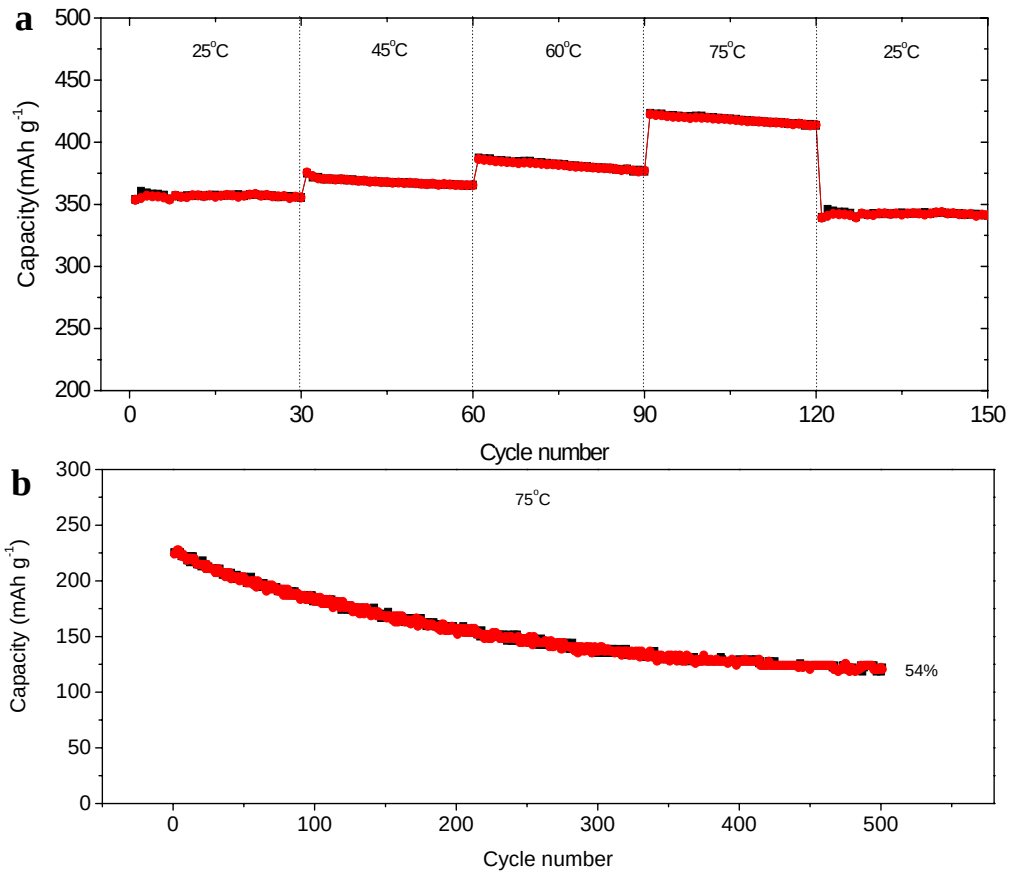

Figure S11. Electrochemical performance of VO_2-graphene architectures with the VO_2 content of 84% under various tempeatures. a, Cycle performance under various temperatures at a current rate of 5C. **b**, Capacity retentions under the highest temperature of 75°C at a current rate of 28C.

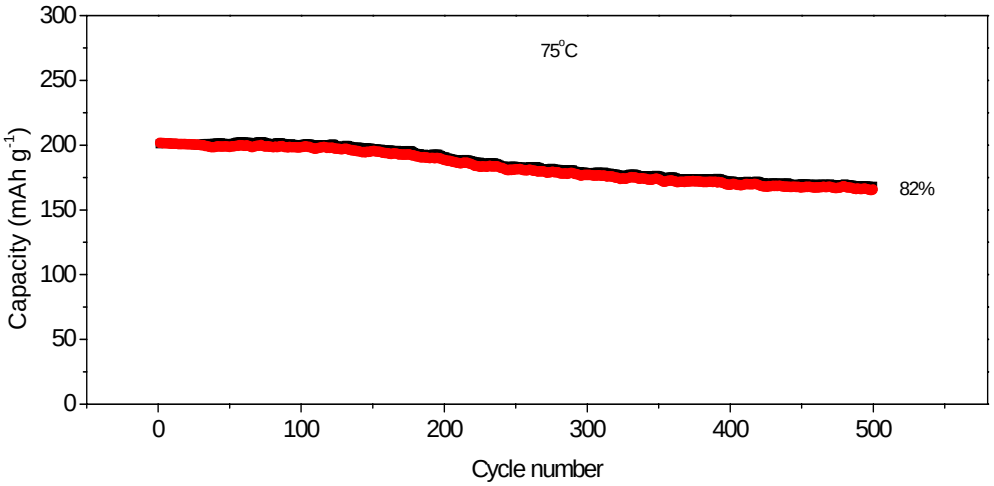

Figure S12. Capacity retention of VO_2-graphene architecture with the VO_2 content of 68% when performing full discharge-charge at a current rate of 28C under the highest temperature of 75°C.